Synthesis of Gold Nanotriangles and Silver Nanoparticles Using *Aloe vera* Plant Extract

S. Prathap Chandran, Minakshi Chaudhary, Renu Pasricha, Absar Ahmad,* and Murali Sastry*,†

Nanoscience Group, Materials Chemistry Division, Biochemical Sciences Division, National Chemical Laboratory, Pune 411008, India

Biogenic gold nanotriangles and spherical silver nanoparticles were synthesized by a simple procedure using *Aloe vera* leaf extract as the reducing agent. This procedure offers control over the size of the gold nanotriangle and thereby a handle to tune their optical properties, particularly the position of the longitudinal surface plasmon resonance. The kinetics of gold nanotriangle formation was followed by UV−vis−NIR absorption spectroscopy and transmission electron microscopy (TEM). The effect of reducing agent concentration in the reaction mixture on the yield and size of the gold nanotriangles was studied using transmission electron microscopy. Monitoring the formation of gold nanotriangles as a function of time using TEM reveals that multiply twinned particles (MTPs) play an important role in the formation of gold nanotriangles. It is observed that the slow rate of the reaction along with the shape directing effect of the constituents of the extract are responsible for the formation of single crystalline gold nanotriangles. Reduction of silver ions by *Aloe vera* extract however, led to the formation of spherical silver nanoparticles of 15.2 nm ± 4.2 nm size.

Introduction

Monodispersity of size and selectivity of shape are two key issues that are the focus of nanoparticle synthesis research. Though monodispersity is very critical for device applications (*1*), the fascinating properties exhibited by anisotropic nanoparticles (*2*) makes shape-selective synthesis exciting. Catalytic properties exhibited by nanocubes of palladium (*3*) and the remarkably different optical properties of gold and silver nanotriangles and nanorods are some examples of exciting shape-dependent properties (*2, 4*). Gold and silver nanotriangles in particular are promising as they could find potential applications in cancer hyperthermia (*5*), as waveguides for electromagnetic radiation (*6*), surface enhanced Raman spectroscopy (SERS) substrates (*7*), and infrared radiation absorbing optical coatings (*8*) to state a few. Consequently, a variety of synthetic procedures leading to planar gold and silver nanostructures have been reported. Methods offering reasonable control over silver nanotriangle edge lengths (*9, 10*) and more recently thickness (*11*) have been reported. These include photochemical transformation of spherical nanoparticles (*9, 10*) or wet chemical synthesis with (*12*) or without templates (*11, 13*). Similar reports for gold, however, are relatively few and more recent. Procedures employing liquid crystal (*14*) and polymer templates (*15*) leading to high yields of planar and triangular gold nanostructures have been reported recently. Solution-based methodologies such as aspartate reduction (*16*) and starch-mediated reduction (*17*) among others (*18*) lead to the production of planar gold nanostructures with reasonable control over their optical properties.

Recently biosynthetic methods employing either biological microorganisms or plant extracts have emerged as a simple and viable alternative to chemical synthetic procedures and physical methods. Following the initial report on intracellular silver nanoparticle formation in *Pseudomonas stutzeri* by Klaus et al (*19*), many reports on syntheses of metal (*20*−*23*) and semiconductor nanoparticles (*24*−*26*) using fungi or bacteria have appeared. In our quest for new eco-friendly "green" methods for the synthesis of noble metal nanoparticles, we have identified fungi (*21, 27*), actinomycetes (*22*), and plant extracts (*29*) for the synthesis of silver (*27*) and gold nanoparticles (*28, 29*). Recently, excellent shape-selective formation of single crystalline triangular gold nanoparticles was observed using the extract of the lemongrass plant (*Cymbopogon flexuosus*) (*5*). These nanostructures possess a strong near-infrared (NIR) absorbance that could be easily tuned by modifying the experimental conditions (*8*). The NIR absorbing properties of the biogenic gold nanotriangles were used to design simple optical coatings for architectural applications (*8*).

In this paper we report on the biological synthesis of single crystalline triangular gold nanoparticles in high yield by the reaction of aqueous chloroaurate ions with the extract of the *Aloe vera* plant. This plant has been used in many medical applications as a result of its antipyretic (*30*), antioxidative (*31*), and cathartic properties (*32*). We show that by varying the percentage of the extract in the reaction medium, the percentage of gold nanotriangles to spherical particles as well as the size of the nanotriangles can be modulated, leading to significant control over the optical properties of the nanoparticulate solution. We believe that slow reduction of the aqueous gold ions along with the shape-directing effects of the constituents of the *Aloe vera* extract play a key role in the formation of the gold nanotriangles. On the other hand, reaction of *Aloe vera* extract with aqueous silver ions yields only spherical nanoparticles. Presented below are the details of the investigation.

* To whom correspondence should be addressed. E-mail: msastry@tatachemicals.com.

† Current address: Tata Chemicals Ltd., Leela Business Park, Andheri (E), Mumbai 400 059, India.

10.1021/bp0501423 CCC: $33.50
Published on Web 03/10/2006

Experimental Section

Materials. Chloroauric acid ($HAuCl_4$) and silver nitrate ($AgNO_3$) were obtained from Aldrich Chemicals and used as received. Ammonia solution about 30% in water was obtained from Merck and used as received. A nylon membrane with a cutoff molecular weight of 3 KDa was procured from Amicon and used as received.

***Aloe vera* Extract Preparation.** A 30 g portion of thoroughly washed *Aloe vera* leaves were finely cut and boiled in 100 mL of sterile distilled water. The resulting extract was used for further experiments.

Synthesis of Gold and Silver Nanoparticles using *Aloe vera* Extract. Different volumes (0.5−4 mL) of the *Aloe vera* leaf extract were added to 6 mL solutions of 10^{-3} M aqueous $HAuCl_4$ separately, and the volume was made up to 10 mL by adding the appropriate amount of deionized water. The effect of the amount of extract on the synthesis of gold nanotriangles was studied by observing the products formed using UV−vis−NIR and transmission electron microscopy (TEM) measurements after allowing the reaction mixture to stand for 30 h, during which time reduction of Au^{3+} in all the reaction mixtures had saturated. Kinetics of the above reduction was studied by following the UV−vis−NIR absorbance and TEM analysis of one particular reaction mixture (10% vol fraction of the extract) as a function of time. The effect of temperature was also studied by performing the reaction at 80 °C. For the synthesis of silver nanoparticles, 2.5 mL of 30% ammonia solution was added to 5 mL of 10^{-2} M $AgNO_3$ solution followed by addition of 5 mL of the *Aloe vera* extract. The concentration of $AgNO_3$ was adjusted to 10^{-3} M by making up the final volume to 50 mL with water. The observation of faint yellow color after 24 h of reaction indicated the formation of silver nanoparticles, which was further characterized by UV−vis absorbance and TEM measurements.

To study the nature of the biomolecules responsible for the formation of gold nanotriangles, the *Aloe vera* extract was fractionated by dialysis using a 3 KDa molecular weight cutoff membrane into two fractions, viz., fraction 1 (biomolecules of MWs less than 3 KDa) and fraction 2 (biomolecules of MWs greater than 3 KDa). This was accomplished by placing the *Aloe vera* extract in a dialysis bag and subjecting the extract to dialysis against pure water. These two fractions were thereafter further reacted with aqueous $HAuCl_4$. The products were characterized using UV−vis−NIR spectroscopy, TEM, and Fourier Transform Infrared (FTIR) spectroscopy analysis.

UV−vis−NIR Absorbance Spectroscopy Studies. UV−vis−NIR spectroscopic measurements of the nanoparticles synthesized were carried out on a JASCO model V-570 dual-beam spectrophotometer operated at a resolution of 1 nm.

TEM Measurements. TEM samples of the gold and silver nanoparticles synthesized using the *Aloe vera* extract were prepared by placing drops of the reaction mixture over carbon-coated copper grids and allowing the solvent to evaporate. TEM measurements were performed on a JEOL model 1200EX instrument operated at an accelerating voltage of 80 kV. For calculating the percentage of gold nanotriangles in a given sample, approximately 150 nanoparticles per sample were taken into account (from images shown here and others). A similar procedure was followed for determination of average edge lengths.

Fourier Transform Infrared Spectroscopy (FTIR) Measurements. FTIR measurements of the *Aloe vera* extract and gold nanoparticles synthesized using the extract deposited on Si(111) substrates were carried out on a Perkin-Elmer FTIR Spectrum One spectrophotometer in the diffuse reflectance mode operating at a resolution of 4 cm^{-1}.

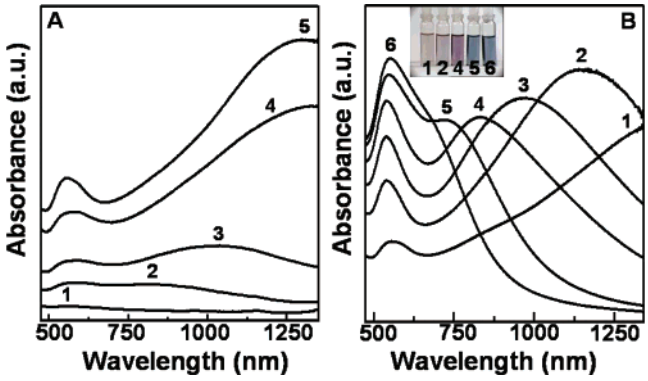

Figure 1. (A) UV−vis−NIR absorption spectra of gold nanoparticles measured during the reaction of 6 mL of 10^{-3} M $HAuCl_4$ with 1 mL of *Aloe vera* extract (final volume of reaction mixture adjusted to 10 mL using deionized water) after 5, 7.5, 8, 9, and 25 h of reaction (curves 1−5, respectively). (B) UV−vis−NIR absorbance spectra of gold nanotriangles formed after 25 h of the reaction of different amounts of *Aloe vera* extract with 6 mL of 10^{-3} M aqueous $HAuCl_4$: 0.5, 1, 1.5, 2, 3, and 4 mL of *Aloe vera* extract (curves 1−6 respectively; final volume of reaction mixtures adjusted to 10 mL using deionized water). The inset in B shows photos of the different nanoparticle solutions after 25 h of the reaction whose labels correspond to spectra shown in the main part of the figure.

Atomic Force Microscope (AFM) Imaging. A VEECO Digital Instruments multimode scanning probe microscope equipped with a Nanoscope IV controller was used for AFM measurements. Samples of *Aloe vera* reduced gold nanoparticles were centrifuged at 1500 rpm for 10 min, and the pellet obtained was washed with deionized water to remove any possible biomass. The pellet was redispersed in a small amount of deionized water by ultrasonication and used for drop coating onto a Si(111) substrate. Samples were analyzed using contact mode AFM using long silicon nitride probes (100 μm). The height data was collected at a scanning frequency of 1 Hz.

EDAX Measurements. EDAX measurements of the *Aloe vera* reduced gold nanoparticles drop coated onto Si(111) wafers were performed on a Leica Stereoscan-440 SEM instrument equipped with a Phoenix EDAX attachment.

Results and Discussion

Addition of *Aloe vera* extract to 10^{-3} M aqueous $HAuCl_4$ solution led to the appearance of a brownish red color in solution after about 5 h of reaction, indicating the formation of gold nanoparticles. The UV−vis−NIR absorption spectrum recorded from this solution shows the characteristic surface plasmon resonance (SPR) band of gold nanoparticles centered at 560 nm (Figure 1A, curve 1). The kinetics of formation of gold nanoparticles was followed by UV−vis−NIR spectroscopy, and the spectra obtained are shown in Figure 1A. It is observed that with the progress of the reaction the absorbance intensity at ca. 560 nm increases monotonically with time while a new band centered at 817 nm appears after about 7.5 h of reaction (curve 2). With time the longer wavelength absorption undergoes a further red shift before stabilizing at 1300 nm after completion of reaction (after 25 h; curves 3−5). These time-dependent features in the UV−vis−NIR spectra are characteristic of aggregated spherical nanoparticles (*33*) or anisotropic nanostructures whose dimensions change with time (*8*). Figure 1B shows the UV−vis−NIR absorbance spectra of gold nanoparticles synthesized using different amounts of *Aloe vera* extract

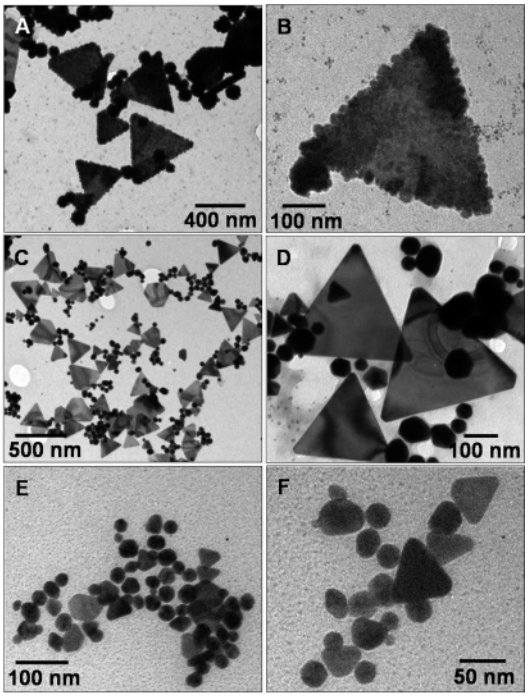

Figure 2. Representative TEM images of gold nanotriangles synthesized using different amounts of *Aloe vera* extract [(A, B) 0.5 mL; (C, D) 1 mL; (E, F) 4 mL] by reaction with 6 mL of 10^{-3} M $HAuCl_4$ (final volume adjusted to 10 mL wherever necessary).

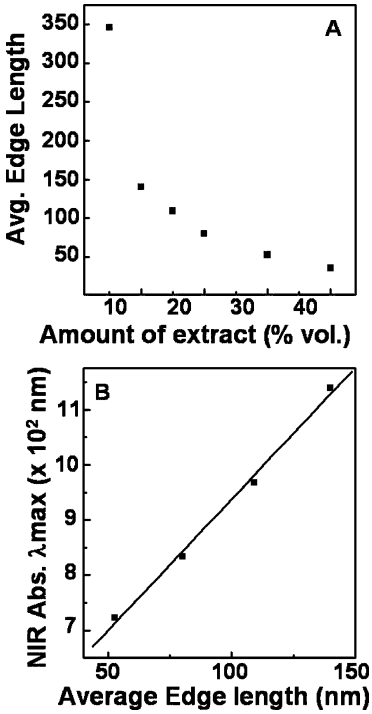

Figure 3. (A) Variation of average edge length of the gold nanotriangles formed in the reaction medium versus the amount of *Aloe vera* extract added (see text for details). (B) Plot of the longitudinal surface plasmon resonance absorbance band wavelength versus the average edge length of the gold nanotriangles synthesized in experiments containing different amounts of *Aloe vera* extract.

recorded after 25 h of the reaction, and the inset shows photographs of the nanoparticle solutions whose labels correspond to the spectra in the main part of the figure. The nanoparticles thus synthesized exhibit two strong absorbance bands; band I centered at ca. 560 nm is a common feature. However, the relative intensity and the position of the second band (band II) that occurs in the NIR region are seen to be a function of the amount of *Aloe vera* extract used in the reaction. It is seen that as the amount of *Aloe vera* extract in the reaction medium increases, band II shifts to smaller wavelengths and weakens in intensity relative to band I (curves 1−6). The corresponding solutions show a large variation in color that ranges from pale pink to dark blue (photos in the inset of Figure 1B) as the amount of the plant extract is increased. It is well-known that rod-shaped and flat gold nanoparticles absorb in the NIR region of the electromagnetic spectrum (*5*, *34*). Such nanostructures exhibit two well-separated absorption bands wherein the low wavelength band centered at ca. 520 nm corresponds to the transverse surface plasmon vibration while the long wavelength component (which could be shifted well into the NIR region) corresponds to the longitudinal surface plasmon absorption (*8*, *34*).

Figure 2 shows representative transmission electron microscopy (TEM) images of the nanoparticles synthesized using different amounts of *Aloe vera* extract. TEM analysis clearly reveals the formation of triangular and a small amount of hexagonal planar gold nanostructures in addition to spherical nanoparticles. Further analysis shows that addition of small amounts (0.5 mL) of *Aloe vera* extract leads to the formation of triangular nanoparticles with larger edge lengths (Figure 2A,B). As the amount of *Aloe vera* extract in the reaction medium is increased to 1 mL, the average edge lengths of the nanotriangles decrease (Figure 2C,D). The same trend is followed on further increase in the amount of *Aloe vera* extract to 4 mL (Figure 2E,F). A systematic edge length analysis of these images and others (Figure 3A) clearly underlines the variation in the size of the nanotriangles. It is well-known that triangular nanoparticles of gold exhibit two characteristic absorption bands referred to as the transverse (out of plane) and longitudinal (in plane) surface plasmon resonance bands. While the out of plane transverse absorbance more or less coincides with the surface plasmon resonance of spherical gold nanoparticles, the in plane surface plasmon band is a strong function of the edge length of the triangles (*4*). This in fact has been found to be the case here with the position of band II showing a direct dependence on the average edge length (Figure 3B) of the triangular nanoparticles. Thus band I and band II in the UV−vis−NIR absorbance spectra can be attributed to the transverse and longitudinal surface plasmon resonance bands, respectively, of the triangular gold nanoparticles being formed. The ability to tune the optical properties of the biogenic gold nanotriangles can be very useful in applications such as cancer cell hyperthermia (*5*) and architectural optical coatings (*8*).

An analysis of the percentage of triangles formed in the reaction medium as a function of varying amounts of the *Aloe vera* extract reveals that more spherical particles are formed with increasing amount of extract (Figure 4A). In one particular case wherein we consider the gold nanoparticles synthesized using 5% *Aloe vera* extract, we see a deviation from the above trend with the percentage of gold nanotriangles being much smaller in comparison with reactions employing higher amounts of extract. This may be attributed to the fact that the gold nanotriangles obtained in this case have a very large average size (edge lengths ∼350 nm) compared to those synthesized using higher amounts of the extract (Figure 4A). The fact that increasing amounts of *Aloe vera* extract leads to an increase in the population of the spherical particles is clearly reflected in the UV−vis−NIR absorbance spectra, which show a relative increase in the intensity of the transverse band in comparison with the longitudinal band (Figure 1B).

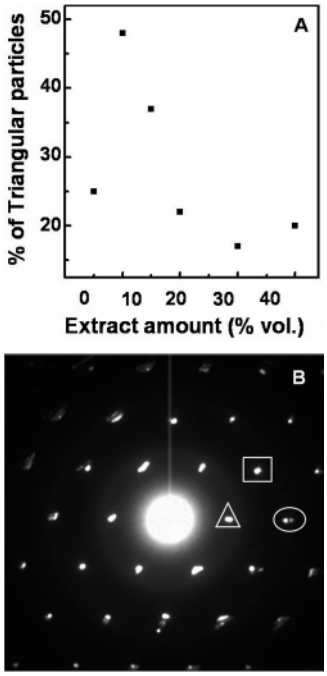

Figure 4. (A) Plot of percentage of triangular nanoparticles formed in the reaction medium versus the amount of *Aloe vera* extract used. (B) Electron diffraction recorded from the triangles shown in Figure 2D. The spots marked using triangles, squares, and ovals correspond to reflections from the 1/3(422), (220), (311) lattice planes of fcc gold.

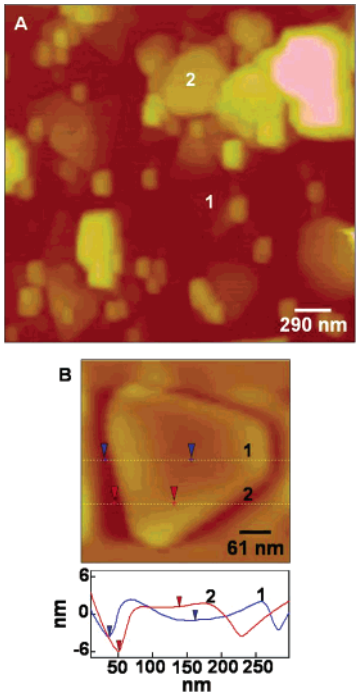

Figure 5. (A) Representative AFM image of *Aloe vera* reduced gold nanoparticles clearly showing triangular (1) and truncated triangular (2) nanoparticles overlapping each other. (B) Contact mode AFM image of one gold nanotriangle. The lower panel shows the topographic height variation along lines 1 and 2 drawn across different areas of the truncated triangle.

The single crystalline nature of the biogenic gold nanotriangles is reflected in the hexagonal nature of the selected area electron diffraction (SAED) spots (Figure 4B) corresponding to one of the triangles shown in Figure 2D. The diffraction spots could be indexed on the basis of the face centered cubic (fcc) structure of gold and are assigned to the 1/3{422}, {220}, and {311} Bragg reflections with lattice spacing of 2.5, 1.44, and 1.23 Å, respectively. This shows that the triangles are highly [111] oriented with the top surface normal to the electron beam (*5*, *35*). The presence of the forbidden 1/3{422} reflection has been explained by Pileni and co-workers as arising as a result of stacking faults in the nanotriangles (*35*) and is a feature common to nanotriangles of gold and silver prepared by a variety of methods (*5*, *9*). Figure 5A shows representative AFM images of the gold nanotriangles prepared using *Aloe vera* extract. A number of triangular and truncated triangular nanoparticles can be seen overlapping each other whose shape is nonetheless visible. Topographic height analysis of one individual truncated triangle is shown in Figure 5B. The thickness of the truncated triangle as measured using two sets of points lying on lines 1 and 2 drawn across different areas of the truncated triangle were found to be 2.6 and 7.9 nm respectively (Figure 5B). Even though the thickness of the gold nanotriangles is not uniform over their surface, the fact that the thickness is much smaller than their edge lengths results in significant separation of the out of plane and in plane surface plasmon vibration modes as observed.

Figure 6A shows the UV−vis−NIR spectra recorded from nanoparticles synthesized using 10% volume fraction of *Aloe vera* extract at a temperature of 80 °C for 30 min (curve 1) along with the control (room temperature reaction, curve 2). For the gold nanoparticles synthesized at elevated temperatures, the longitudinal plasmon resonance band is drastically blue shifted to 719 nm from 1140 nm as in the room temperature sample. TEM analysis of the gold nanoparticles obtained at elevated temperatures shows predominantly aggregated structures (Figure 6B) and very few spherical particles, thus accounting for the observed absorbance profile (Figure 6A, curve 1). The SAED pattern (inset of Figure 6B) of this sample shows that the gold nanostructures are crystalline and randomly oriented. The electron diffraction pattern could be indexed on the basis of the fcc structure of gold. In a recent report, aspartate reduction of gold ions has been found to yield single crystalline

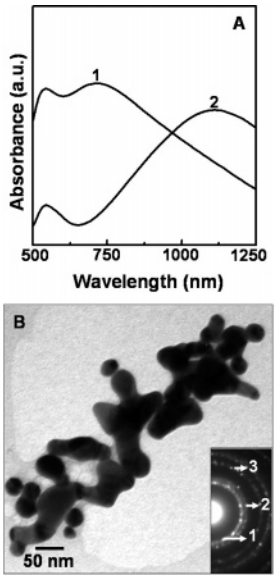

Figure 6. (A) UV−vis−NIR absorption spectra of nanoparticles synthesized by reacting 1 mL of *Aloe vera* extract with 6 mL of 10^{-3} M $HAuCl_4$ solution (final volume adjusted to 10 mL) at 80 °C (curve 1) and at room temperature (curve 2). (B) Representative TEM image of gold nanoparticles formed in the solution corresponding to curve 1 in A. The inset shows the electron diffraction pattern of the particles in the main part of the image. Rings 1, 2, and 3 arise due to reflections from the (111), (200), and (220) lattice planes of fcc gold.

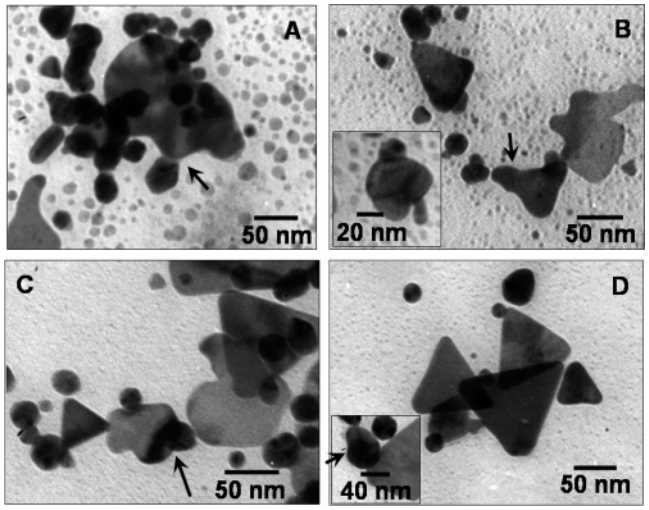

Figure 7. Representative TEM images of samples prepared after (A) 1.5, (B) 2, (C) 3.5, and (D) 7 h following start of the reaction, showing gold nanoparticles that have formed on adding 1 mL of *Aloe vera* extract to 6 mL of 10^{-3} M aqueous $HAuCl_4$ solution (final volume adjusted to 10 mL). The arrows indicate MTPs undergoing shape transformation.

triangular and hexagonal structures under room temperature conditions (*16*). The same reaction when carried out under boiling conditions did not yield triangular and hexagonal structures (*36*). These observations highlight the importance that slow reaction conditions play in the growth of anisotropic particles of single crystalline nature.

Xia and co-workers have observed that nanorods evolve from multiply twinned particles (MTPs) as a result of anisotropic growth caused by certain shape-directing agents (*37*). Here too we speculate that MTPs play a major role in directing the morphology of gold nanotriangles. The formation of the gold nanotriangles was studied by analyzing samples of the nanoparticulate solution during the course of the reaction. It can be clearly seen that during the initial stages of the reaction (after 1.5 h, Figure 7A) there is a large population of small particles, which are spherical in shape. Accompanying these are the larger particles that are sintering, leading to the formation of anisotropic structures. The arrow clearly indicates a MTP participating in such a sintering. After 2 h of reaction (Figure 2B) the formation of structures that resemble a triangular shape was observed. The inset in Figure 2B clearly shows an MTP undergoing a shape transformation. After 3.5 h of reaction, the population of the triangles shows an increase and is accompanied by continued shape transformation of the MTPs as indicated in Figure 2C. After 7 h of reaction, well-defined gold nanotriangles form. The inset again highlights the role that MTPs play in the formation of nanotriangles. It has been shown that slow reduction and thus slow crystallization leads to the formation of MTPs as a result of their inherent stability (*37*). It is quite possible that MTPs that initially form under the slow reaction conditions undergo shape transformation and evolve into gold nanotriangles as a result of the shape-directing effect of the constituents of the *Aloe vera* extract. A recent study has been reported that the presence of defects such as twin planes direct the formation of anisotropic metal nanostructures such as planar triangles, hexagons, and rods (*38*). This observation further supports our view that MTPs play a major role in the formation of gold nanotriangles. Moreover it has been observed by Wang and co-workers that the difference in the growth rates of the various crystallographic planes could also lead to the evolution of the morphology of the nanparticles (*39*).

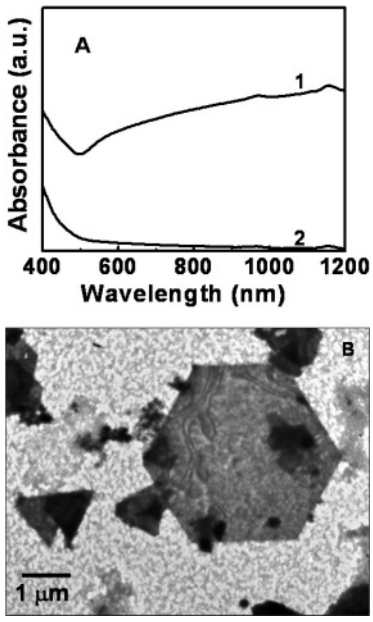

Figure 8. (A) UV−vis−NIR absorbance spectra of solutions obtained on reacting 6 mL of 10^{-3}M aqueous $HAuCl_4$ with 1 mL each of fraction 1 (curve 1) and fraction 2 (curve 2) of the *Aloe vera* extract (final volume adjusted to 10 mL). (B) Representative TEM image of the nanoparticles formed on reacting 1 mL of fraction 1 with 5 mL of 10^{-3} M aqueous $HAuCl_4$ (final volume adjusted to 10 mL).

To study the biomolecules responsible for the formation of gold nanotriangles, the *Aloe vera* extract was separated using a 3 kDa nylon dialysis bag. Fraction 1 with molecular weight less than 3 kDa and fraction 2 with molecular weight greater than 3 kDa were separated. It was observed that only fraction 1 causes reduction of the gold ions, leading to the formation of gold nanoparticles. Figure 8A shows the UV−Vis−NIR absorbance spectra of gold nanoparticles that have been synthesized on reacting aqueous $HAuCl_4$ with fraction 1 of the *Aloe vera* extract (curve 1, Figure 8A). The presence of a very broad surface plasmon resonance indicates the reduction of gold ions. The formation of gold nanotriangles is further verified using TEM measurements. Very large triangular and hexagonal gold nanotriangles are seen in addition to smaller nanoparticles (Figure 8B). The absence of any distinct absorbance peak in the reaction mixture when fraction 2 was reacted with gold ions was used to conclude that the reducing and shape-directing agents that cause formation of the nanotriangles have a molecular weight less than 3 kDa.

FTIR analysis was used for the characterization of the extract and the resulting nanoparticles (Figure 9A). The FTIR spectrum of the *Aloe vera* extract (curve I, Figure 9A) shows bands at 1731 and 1588 cm^{-1} along with an intense broad absorbance at 3320 cm^{-1} (not shown here). The band at 1731 cm^{-1} (peak 1, Figure 9A) is characteristic of stretching vibrations of the carbonyl functional group in ketones, aldehydes, and carboxylic acids. The 1588 cm^{-1} (peak 2, Figure 9A) band can be assigned to aromatic C−C skeletal vibrations. The band at 3320 cm^{-1} is characteristic of the hydroxyl functional group in alcohols and phenolic compounds. The FTIR spectrum of fraction 1 of the *Aloe vera* extract is shown in curve II of Figure 9A. Components of fraction 1, however, possess vibrational peaks at 1770 (peak 3, Figure 9A) and 1710 cm^{-1} (peak 4, Figure 9A) apart from a peak at 1120 cm^{-1} (peak 5, Figure 9A). These indicate the presence of carbonyl and alcoholic groups in the components of reaction 1. After reaction with gold ions (curve III), however, an enhancement in the signal corresponding to a carbonyl group

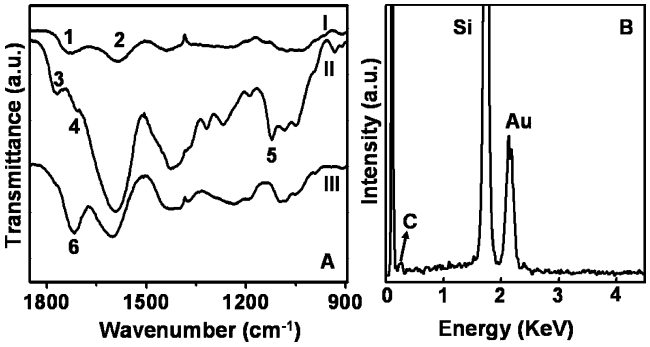

Figure 9. (A) FTIR spectra of the *Aloe vera* extract (curve I) and fraction 1 of the same extract (curve II, see text for details). FTIR spectra of gold nanoparticles (curve III) synthesized by adding 1 mL of fraction 1 of *Aloe vera* extract to 6 mL of 10^{-3} M aqueous $HAuCl_4$ solution (final volume adjusted to 10 mL). (B) Spot profile EDAX spectrum recorded from gold nanotriangles prepared by addition of 1 mL of *Aloe vera* extract to 6 mL of 10^{-3} M aqueous $HAuCl_4$ solution (final volume adjusted to 10 mL).

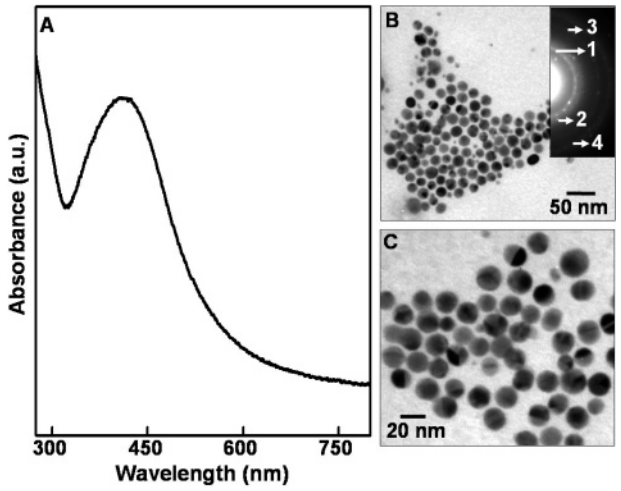

Figure 10. (A) UV−vis absorption spectrum of silver nanoparticles prepared using *Aloe vera* extract. (B, C) Representative TEM images of silver nanoparticles synthesized using *Aloe vera* extract. The inset in B shows the electron diffraction pattern recorded from the particles shown in B. Rings 1, 2, 3, and 4 arise due to reflections from (111), (200), (220), and (311) lattice planes of fcc silver, respectively.

as in aldehydic or ketonic components is observed (peak 6, Figure 9A). The absence of the 1120 cm^{-1} signal in the reaction mixture indicates that the reduction of the gold ions is coupled to the oxidation of the alcoholic component of fraction 1 of *Aloe vera* extract. This observation is similar to our previous report on gold nanotriangle synthesis using lemon grass extract wherein carbonyl groups were found to play an important role in the stabilization and capping of the gold nanotriangles (*5*). Spot profile EDAX spectra recorded from the gold nanotriangles (Figure 9B) show a strong Au signal along with a weak carbon peak, which originates from the biomolecules that are bound to the surface of the gold nanotriangles.

Silver nanoparticles were also synthesized using the *Aloe vera* extract from silver nitrate. The reaction proceeded only in the presence of ammonia, which facilitates the formation of a soluble silver complex (diamminesilver(I) chloride) that then facilitates the reduction. The reaction mixture turned pale yellow after 24 h of reaction and exhibited an absorbance peak at 410 nm (Figure 10A) characteristic of silver nanoparticles due to its surface plasmon absorbance. TEM analysis reveals that the silver nanoparticles are predominantly spherical (Figure 10B,C), and the average size of the spherical silver nanoparticles was estimated to be 15.2 ± 4.2 nm. The inset in Figure 10B shows the selected area electron diffraction pattern recorded from the silver nanoparticles. The ring-like diffraction pattern indicates that the particles are crystalline; the diffraction rings could be indexed on the basis of the fcc structure of silver. Unlike reduction of chloroaurate ions that lead to the formation of a large percentage of nanotriangles, such shape control is not exhibited during the formation of silver nanoparticles. Although a more detailed study is required to fully understand this difference in nanoparticle morphology, we speculate that it could be due to the differences in binding of the biomolecules with the surface of silver nanoparticles. Weaker binding of these biomolecules with nascent silver nanocrystals could lead to isotropic growth of the crystals and thus formation of spherical particles.

Conclusions

The biological synthesis of gold nanotriangles using *Aloe vera* extract provides a simple and efficient route for the synthesis of nanomaterials with tunable optical properties directed by particle shape. The size of the gold nanotriangles can be easily varied from 50 to 350 nm by merely adjusting the amount of *Aloe vera* extract used in the gold ion reduction. The slow rate of reduction of gold ions by the biomolecules aided by the shape-directing ability of the carbonyl compounds of the *Aloe vera* extract are believed to be responsible for the formation of the single crystalline gold nanotriangles. TEM analysis of samples prepared at different time intervals after the onset of the reaction proves the evolution of MTPs into flat triangular nanostructures by way of shape transformation. The strong NIR absorbance of the gold nanotriangles and the flexibility with which this could be tuned could find interesting applications in cancer hyperthermia and optical coatings (*5*, *8*).

Acknowledgment

S.P.C. thanks Council of Scientific and Industrial Research (CSIR), Government of India for financial assistance.

References and Notes

(1) Fendler, J. H.; Meldrum, F. C. Colloid chemical approach to nanostructured materials. *Adv. Mater.* **1995**, *7*, 607−632.
(2) El-Sayed, M. A. Some interesting properties of metals confined in time and nanometer space of different shapes. *Acc. Chem. Res.* **2001**, *34*, 257−264.
(3) Shi, A.-C.; Masel, R. I. The effects of gas adsorption on particle shapes in supported platinum catalysts. *J. Catal.* **1989**, *120*, 421−431.
(4) Kelly, K. L.; Coronado, E.; Zhao, L. L.; Schatz, G. C. The optical properties of metal nanoparticles: The influence of size, shape, and dielectric environment. *J. Phys. Chem. B* **2003**, *107*, 668−677.
(5) Shankar, S. S.; Rai, A.; Ankamwar, B.; Singh, A.; Ahmad, A.; Sastry, M. Biological synthesis of triangular gold nanoprisms. *Nat. Mater.* **2004**, *3*, 482−488.
(6) Maier, S. A.; Brongersma, M. L.; Kik, P. G.; Meltzer, S.; Requicha, A. A. G.; Atwater, H. A. Plasmonics—a route to nanoscale optical devices. *Adv. Mater.* **2001**, *13*, 1501−1505.
(7) Dick, L. A.; McFarland, A. D.; Haynes, C. L.; Van Duyne, R. P. Metal film over nanosphere (MFON) electrodes for Surface-Enhanced Raman Spectroscopy (SERS): Improvements in surface nanostructure stability and suppression of irreversible loss. *J. Phys. Chem. B* **2002**, *106*, 853−860.
(8) Shankar, S. S.; Rai, A.; Ahmad, A.; Sastry, M. Controlling the optical properties of lemongrass extract synthesized gold nanotriangles and potential application in infrared-absorbing optical coatings. *Chem. Mater.* **2005**, *17*, 566−572.
(9) Jin, R.; Cao, Y.; Mirkin, C. A.; Kelly, K. L.; Schatz, G. C.; Zheng, J. G. Photoinduced conversion of silver nanospheres to nanoprisms. *Science* **2001**, *294*, 1901−1903.

(10) Jin, R.; Cao, Y. C.; Hao, E.; Metraux, G. S.; Schatz, G. C.; Mirkin, C. A. Controlling anisotropic nanoparticle growth through plasmon excitation. *Nature* **2003**, *425*, 487−490.
(11) Metraux, G. S.; Mirkin, C. A. Rapid thermal synthesis of silver nanoprisms with chemically tailorable thickness. *Adv. Mater.* **2005**, *17*, 412−415.
(12) Hao, E.; Kelly, K. L.; Hupp, J. T.; Schatz, G. C. Synthesis of silver nanodisks using polystyrene mesospheres as templates. *J. Am. Chem. Soc.* **2002**, *124*, 15182−15183.
(13) Pastoriza-Santos, I.; Liz-Marzon, L. M. Synthesis of silver nanoprisms in DMF. *Nano Lett.* **2002**, *2*, 903−905.
(14) Wang, L.; Chen, X.; Zhan, J.; Chai, Y.; Yang, C.; Xu, L.; Zhuang, W.; Jing, B. Synthesis of gold nano- and microplates in hexagonal liquid crystals. *J. Phys. Chem. B* **2005**, *109*, 3189−3194.
(15) Kim, J.; Cha, S.; Shin, K.; Jho, J. Y.; Lee, J. C. Preparation of gold nanowires and nanosheets in bulk block copolymer phases under mild conditions. *Adv. Mater.* **2004**, *16*, 459−464.
(16) Shao, Y.; Jin, Y.; Dong, S. Synthesis of gold nanoplates by aspartate reduction of gold choride. *Chem. Commun.* **2004**, 1104−1105.
(17) Sarma, T. K.; Chattopadhyay, A. starch-mediated shape-selective synthesis of Au nanoparticles with tunable longitudinal plasmon resonance. *Langmuir* **2004**, *20*, 3520−3524.
(18) Sau, T. K.; Murphy, C. J. Room temperature, high-yield synthesis of multiple shapes of gold nanoparticles in aqueous solution. *J. Am. Chem. Soc.* **2004**, *126*, 8648−8649.
(19) Klaus, T.; Joerger, R.; Olsson, E.; Granqvist, C. G. Silver-based crystalline nanoparticles, microbially fabricated. *Proc. Natl. Acad. Sci. U.S.A.* **1999**, *96*, 13611−13614.
(20) Gardea-Torresdey, J. L.; Parsons, J. G.; Gomez, E.; Peralata-Videa, J.; Troinai, H. E.; Santiago, P.; Yacaman, M. J. Formation and growth of Au nanoparticles inside live *Alfalfa* plants. *Nano Lett.* **2002**, *2*, 397−401.
(21) Mukherjee, P.; Ahmad, A.; Mandal, D.; Senapati, S.; Sainkar, S. R.; Khan, M. I.; Ramani, R.; Pasricha, R.; Ajayakumar, P. V.; Alam, M.; Sastry, M. Bioreducion of $AuCl^{4-}$ ions by the fungus, *Verticillium* sp. and surface trapping of the gold nanoparticles formed. *Angew. Chem., Int. Ed.* **2001**, *40*, 3585−3588.
(22) Ahmad, A.; Senapati, S.; Khan, M. I.; Kumar, R.; Sastry, M. Extracellular biosynthesis of monodisperse gold nanoparticles by a novel extremophilic actinomycete, *Thermomonospora* sp. *Langmuir* **2003**, *19*, 3550−3553.
(23) Brown, S.; Sarikaya, M.; Johnson, E. A genetic analysis of crystal growth. *J. Mol. Biol.* **2000**, *299*, 725−735.
(24) Dameron, C. T.; Resse, R. N.; Mehra, R. K.; Kortan, A. P.; Caroll, P. J.; Steigerwald, M. L.; Brus, L. E.; Winge, D. R. Biosynthesis of cadmium sulphide quantum semiconductor crystallites. *Nature* **1989**, *338*, 596;
(25) Labrenz, M.; Druschel, G. K.; Thomsen-Ebert, T.; Gilbert, B.; Welch, S. A.; Kemner, K. M.; Logan, G. A.; Summons, R. E.; Stasio, G. D.; Bond, P. L.; Lai, B.; Kelly, S. D.; Banfield, J. F. Formation of sphalerite (ZnS) deposits in natural biofilms of sulfate-reducing bacteria. *Science* **2000**, *290*, 1744−1747.
(26) Ahmad, A.; Mukherjee, P.; Mandal, D.; Senapati, S.; Khan, M. I.; Kumar, R.; Sastry, M. Enzyme mediated extracellular synthesis of CdS nanoparticles by the fungus *Fusarium oxysporum. J. Am. Chem. Soc.* **2002**, *124*, 12108−12109.
(27) Mukherjee, P.; Ahmad, A.; Mandal, D.; Senapati, S.; Sainkar, S. R.; Khan, V; Parishcha, R.; Ajaykumar, P. V.; Alam, M.; Kumar, R.; Sastry, M. Fungus-mediated synthesis of silver nanoparticles and their immobilization in the mycelial matrix: A novel biological approach to nanoparticle synthesis. *Nano Lett.* **2001**, *1*, 515−519.
(28) Shankar, S. S.; Ahmad, A.; Sastry, M. Geranium leaf assisted biosyntheis of silver nanoparticles. *Biotechnol. Prog.* **2003**, *19*, 1627−1631.
(29) Shankar, S. S.; Ahmad, A.; Pasricha, R.; Sastry, M. Bioreduction of chloroaurate ions by geranium leaves and its endophytic fungus yields gold nanoparticles of different shapes**.** *J. Mater. Chem.* **2003**, *13*, 1822−1826.
(30) Shin, K. H.; Woo, W. S.; Lim, S. S.; Shim, C. S.; Chung, H. S.; Kennely, E. J.; Kinghorn, A. D. Elgonica-dimers A and B, two potent alcohol metabolism inhibitory constituents of *Aloe arborescens*. *J. Nat. Prod.* **1997**, *60*, 1180−1182.
(31) Umano, K.; Nakahara, K.; Shoji, A.; Shibamoto, T. Aroma chemicals isolated and identified from leaves of *Aloe arborescens* Mill. Var. *natalensis* Berger. *J. Agric. Food Chem.* **1999**, *47*, 3702−3705.
(32) Saccu, D.; Bagoni, P.; Procida, G. J. Aloe exudate: Characterization by reversed phase HPLC and headspace GC−MS. *J. Agric. Food Chem.* **2001**, *49*, 4526−4530.
(33) Shipway, A. N.; Lahav, M.; Gabai, R.; Willner, I. Investigations into the electrostatically induced aggregation of Au nanoparticles. *Langmuir* **2000**, *16*, 8789−8795.
(34) Link, S.; El-Sayed, M. A. Optical properties and ultrafast dynamics of metallic nanocrystals. *Annu. Rev. Phys. Chem.* **2003**, *54*, 331−366.
(35) Germain, V.; Li, J.; Ingert, D.; Wang, Z. L.; Pileni, M. P. Stacking faults in formation of silver nanodisks. *J. Phys. Chem. B* **2003**, *107*, 8717−8720.
(36) Mandal, S.; Selvakannan, PR.; Phadtare, S.; Pasricha, R.; Sastry, M, Synthesis of a stable gold hydrosol by the reduction of chloroaurate ions by the amino acid, asparitic acid. *Proc. Indian Acad. Sci. (Chem. Sci.)* **2002**, *114*, 513−520.
(37) Wiley: B.; Sun, Y.; Mayers, B.; Xia, Y. Shape controlled synthesis of metal nanostructures: The case of silver. *Chem. Eur. J.* **2005**, *11*, 454−463.
(38) Lefton, C.; Sigmud, W. Mechanisms controlling crystal habits of gold and silver colloids. *Adv. Funct. Mater.* **2005**, *15*, 1197−1208.
(39) Wang, Z. L. Transmission electron microscopy of shape-controlled nanocrystals and their assemblies. *J. Phys. Chem. B* **2000**, *104*, 1153−1175.

Accepted for publication January 26, 2006.

BP0501423